DOT/FAA/AR-10/20

Air Traffic Organization
NextGen & Operations Planning
Office of Research and
Technology Development
Washington, DC 20591

Evaluation of Delaminations and Impact Damage in Composites Using the A_0 Lamb Mode

January 2011

Final Report

This document is available to the U.S. public through the National Technical Information Services (NTIS), Springfield, Virginia 22161.

This document is also available from the Federal Aviation Administration William J. Hughes Technical Center at actlibrary.tc.faa.gov.

U.S. Department of Transportation
Federal Aviation Administration

NOTICE

This document is disseminated under the sponsorship of the U.S. Department of Transportation in the interest of information exchange. The United States Government assumes no liability for the contents or use thereof. The United States Government does not endorse products or manufacturers. Trade or manufacturer's names appear herein solely because they are considered essential to the objective of this report. The findings and conclusions in this report are those of the author(s) and do not necessarily represent the views of the funding agency. This document does not constitute FAA certification policy. Consult your local FAA aircraft certification office as to its use.

This report is available at the Federal Aviation Administration William J. Hughes Technical Center's Full-Text Technical Reports page: actlibrary.tc.faa.gov in Adobe Acrobat portable document format (PDF).

Technical Report Documentation Page

1. Report No.	2. Government Accession No.	3. Recipient's Catalog No.
DOT/FAA/AR-10/20		

4. TITLE AND SUBTITLE	5. Report Date
EVALUATION OF DELAMINATIONS AND IMPACT DAMAGE IN COMPOSITES USING THE A_0 LAMB MODE	January 2011
	6. Performing Organization Code
7. Author(s)	8. Performing Organization Report No.
G. Petculescu, S. Krishnaswamy, and J. D. Achenbach	
9. Performing Organization Name and Address	10. Work Unit No. (TRAIS)
Center for Quality Engineering and Failure Prevention, Northwestern University Rm 327, 2137 Tech Drive Evanston, IL 60208, USA	11. Contract or Grant No.
12. Sponsoring Agency Name and Address	13. Type of Report and Period Covered
U.S. Department of Transportation Federal Aviation Administration Air Traffic Organization NextGen & Operations Planning Office of Research and Technology Development Washington, DC 20591	14. Sponsoring Agency Code AMN-115

15. Supplementary Notes

The Federal Aviation Administration Airport and Aircraft Safety R&D Division Technical Monitor was David Westlund.

16. Abstract

This research examined the development of structural health monitoring (SHM) sensors for detection of delaminations in composite structures. The lowest antisymmetric Lamb mode, A_0, excited in a zone with minimal dispersion, at a wavelength of 4.5 mm, was used in two tests: (1) the detection and size estimation of simulated mid-plane delaminations in woven, quasi-isotropic, carbon-epoxy composites and (2) the evaluation of impact damage in unidirectional, cross-ply, carbon-epoxy composites. The mid-plane delaminations were simulated by circular inserts of various types and sizes introduced in the panel mid-plane during fabrication. The impact was administered using a 1-inch-radius impactor with controlled energy. The A_0 propagation characteristics in the composite, with and without defects, were analyzed. The change in the mode's group velocity was used as a qualitative damage indicator while the accumulated time delay of the traveling ultrasonic pulse was used for quantitative size estimation of the delaminations. The results were repeatable; suggesting that time delay is a reliable damage parameter for quantitative monitoring of delaminations and impact damage in composites. The transducers used to excite and detect the Lamb waves were array-type transducers able to select a specific mode. The transducers' low profile, malleability, minimal cost, and low Q factor are important features for sensors intended to be used in SHM. While the laboratory test results were promising, future work in this area would need to be scaled up by considering more realistic damage sizes as well as more representative composite structure used in real aircraft designs. Addressing these issues would bring SHM technology closer to the necessary level so that it may be used as a tool for monitoring damage accumulation in composite aircraft structure.

17. Key Words	18. Distribution Statement
Lamb waves, Delamination, Impact damage, Graphite-epoxy composites, PVDF transducer	This document is available to the U.S. public through the National Technical Information Service (NTIS), Springfield, Virginia 22161. This document is also available from the Federal Aviation Administration William J. Hughes Technical Center at actlibrary.tc.faa.gov.

19. Security Classif. (of this report)	20. Security Classif. (of this page)	21. No. of Pages	22. Price
Unclassified	Unclassified	29	

Form DOT F 1700.7 (8-72) Reproduction of completed page authorized

ACKNOWLEDGEMENTS

The authors thank Lamia Salah, National Institute for Aviation Research, for specially preparing the cross-ply specimen and Kirk Rackow, Sandia National Laboratories, for providing the woven composite panel. The authors thank John Townsley, Boeing Phantom Works, for information on the material properties of woven composites. The authors are thankful to Sang-Woo Choi, Northwestern University, for providing the C-scan images.

TABLE OF CONTENTS

		Page
EXECUTIVE SUMMARY		xi
1.	INTRODUCTION	1
2.	METHODOLOGY	1
2.1	Specimens	2
2.2	Lamb Waves	3
2.3	Transducers	4
2.4	Experimental Procedure	7
3.	DETECTION OF ARTIFICIAL DELAMINATIONS	8
3.1	Modal Purity	8
3.2	Results for Artificial Delaminations	9
3.2.1	Scan of 3.7-mm-Thick Side, $[0/45/-45/90]_{2S}$	10
3.2.2	Scan of 5.6-mm-Thick Side, $[0/45/-45/90]_{3S}$	11
3.3	Analysis	12
3.4	Discussion	14
4.	DETECTION OF IMPACT DAMAGE	15
4.1	Modal Purity	15
4.2	Results for Impact Damage	15
4.3	Discussion	16
5.	CONCLUSION	17
6.	REFERENCES	17

LIST OF FIGURES

Figure		Page
1	Specimen I, a Carbon-Epoxy, Plain-Weave, Quasi-Isotropic Composite Panel Reference Standard	2
2	Numerically Calculated Phase Velocity Dispersion Curves for Lamb Waves in the Composite Materials Investigated, (a) Specimen I and (b) Specimen II	4
3	Top and Expanded Cross-Section Views of the Transducer	5
4	Spatial Distribution Spectrum of the Finger Electrodes as a Function of the Wave Number $k = 2\pi/\lambda_0$	6
5	Two Different Modes Excited by the Same Pair of Transducers (λ_0 = 4.5 mm) at two Different Frequencies in the Cross-Ply Specimen	7
6	The Experimental Setup	7
7	Propagation Characteristics of the Excited Mode Along the x Direction of the Composite Panel	8
8	Type I Scan	9
9	Type I Scan of the row of Teflon Inserts (from 1.5 to 0.25 in.) on the 3.7-mm Side of the Panel	10
10	Type I Scan Time Delay Measurement of the 4-Ply Pillow Inserts on the 3.7-mm Side of the Panel	10
11	Type II Scan Time Delay Measurement on the 3.7-mm Side of the Panel	11
12	Type I Scan Time Delay Measurement of the Teflon Inserts Row (sizes from 1.5 to 0.25 in.) on the 5.6-mm Side of the Panel	12
13	Type II Scan Time Delay Measurement of the Column With 0.75-Inch Inserts of Different Types on the 5.6-mm Side of the Panel	12
14	Geometry Used for Calculating the Velocity at Half Plate From the Observed Time Delay and the Defect Diameter	13

15 Time Traces of the Received Signal in the 22-J Impact Test and the Amplitude and Time Delay of the A_0 Pulse Measured as a Function of the Number of Impacts 16

16 Ultrasonic C-Scan Image of the Impacted Cross-Ply Coupon in the Damaged Area at the Location of the two Hit Points (28 J and 22 J) 16

LIST OF TABLES

Table		Page
1	Material Properties of a Layer Used in Calculating the Dispersion Curves of the two Specimens Used in the Experiments	4
2	Defect Diameter Φ Calculated From the Time Delay Measurements for the 4-Ply Pillow Defects and the 16-Ply Teflon Defects	14

LIST OF SYMBOLS AND ACRONYMS

λ_0	Smallest wavelength for a given mode
fD	Frequency-thickness product
mm/µs	Millimeters per microsecond
A_0	Lowest antisymmetric Lamb wave mode
S_0	First symmetric Lamb mode wave
AC	Alternating current
MHz·mm	MegaHertz millimeters
NDE	Nondestructive Evaluation
PVDF	Polyvinylidene fluoride
PZT	Lead Zirconate Titanate
RF	Radio frequency
SHM	Structural Health Monitoring
S/N	Signal-to-noise

EXECUTIVE SUMMARY

Structural degradation, whether engendered by inherent material aging due to the environment and service loads (fatigue, corrosion, etc.) or by unpredictable external effects (impact, etc.) is inevitable. Structural health monitoring (SHM) systems can help prevent structural failure of safety-critical structures that cannot be allowed to fail in service. An intelligent health monitoring network should include a network of sensors to monitor several critical parameters that affect structural integrity. The sensors need to function in an autonomous fashion and conform to stringent restrictions of size, weight, and power consumption. It is also desirable to integrate the sensors with wireless telemetry for data uplink to a central processing unit. Where possible, the sensors should be either passive or remotely powered.

An absolute requirement for the successful development of an SHM system is a network of simple but accurate sensors. Because these devices need to be permanently attached to parts of a complex structure, they need to be unobtrusive, light, and flexible. Industry, national laboratories, and universities have performed significant work in the area of intelligent SHM systems. This work includes the use of fiber-optic sensors, remote monitoring of electrical continuity of thin crack wires, embedded microsensors, embedded piezoelectric sensors, and wireless condition-monitoring systems. Conventional piezoelectric transducers for Lamb wave generation are unsuitable, given their size, cost, and bandwidth. Lamb waves are inherently dispersive. This property can be advantageously channeled if independent Lamb modes can be excited and detected. This can be realized by using narrow-band sensors.

In this research, a group delay measurement technique was developed using modally selective Lamb wave transducers for the detection and sizing of delaminations in unidirectional and cross-ply composites. Unlike amplitude or energy-based Lamb wave methods, this method is insensitive to transducer coupling. Specifically, modally selective array transducers were used to generate the lowest antisymmetric A_0 Lamb mode in a zone with minimal dispersion. The change in the modal group velocity was used as a damage indicator while the accumulated time delay of the traveling ultrasonic wavepacket was used for size estimation of the delaminations. The results were repeatable, suggesting time delay was a reliable damage parameter for quantitative monitoring of delaminations and impact damage in composites.

1. INTRODUCTION.

As laminated graphite-epoxy composites are more frequently used for safety-critical, load-carrying structures, nondestructive evaluation (NDE) of their structural integrity is becoming increasingly important. Ultrasonic techniques, such as C-scans and Lamb wave methods, are suitable methods for NDE of composite laminates. Lamb wave methods, in particular, have proven to be efficient tools for inspecting plate- and pipe-like components [1-4]. Lamb waves propagate over extended distances in materials including composites. Therefore, they can be used to probe large areas of structures, through their entire thickness. Lamb waves are easily excited and detected by conventional piezoelectric transducers. Experimental and theoretical aspects of the propagation of Lamb waves in stratified media with complex geometries, with direct applications to composites, have been analyzed in detail [5]. Changes in the amplitude or energy of transmitted ultrasonic waves have been suggested as potential ways to identify underlying defects, when structural integrity is evaluated. However, monitoring only the amplitude and/or the total energy of a transmitted or reflected signal may not be a reliable method for damage identification. Variability in the coupling and the sensitivity of transducers can induce changes in the amplitude and energy of the signal that are often comparable with those caused by damage.

In contrast to amplitude or energy measurements, velocimetric methods [6] that track changes in ultrasonic velocities due to variations in geometry or material properties can be used to reliably detect damage. The effect of the variation of Lamb wave velocities with thickness has been previously used to detect corroded areas in metals [7 and 8] and to identify delaminated zones in glass-reinforced composites [9]. In this research, changes in the group velocities of the lowest antisymmetric Lamb wave mode, A_0, were used to detect and estimate damage. The first experiment was a systematic study of detection and size estimation of artificial mid-plane delaminations in woven, quasi-isotropic, carbon-epoxy composites. This material is of interest because of its industrial applications as a versatile composite with improved impact resistance. The second experiment focused on the detection of real delaminations created by impact on cross-ply, carbon-epoxy composites. To facilitate a simple and direct way to monitor velocity changes, array-type modally selective Lamb wave transducers were used to effectively generate and receive the A_0. The transducers are made of polyvinylidene fluoride (PVDF) film and are easy to fabricate. The transducers are very thin and malleable and are inexpensive. These properties make the sensors particularly suitable for online structural health monitoring (SHM), in which numerous sensors have to be permanently installed on a structural component.

2. METHODOLOGY.

A_0, excited in a frequency domain with low dispersion, was used for detection and sizing of delaminations. Two types of delaminations were investigated. Mid-plane delaminations were simulated through inserts of various types and sizes, which were introduced in a quasi-isotropic woven composite panel during fabrication. The interaction of the ultrasonic pulse with such defects produces some wave scattering, possible mode conversion, and variations in the modal group velocity due to thickness or material property changes in the delaminated zone. The recorded changes in the phase of the received time traces of waves propagating through zones with and without delaminations were the basis for the quantitative detection method used here. The second type of delamination was created by impacting a cross-ply composite panel. The

low-velocity impact produced delaminations distributed at multiple interfaces throughout the thickness of the panel. Matrix cracking and fiber breakage were also present. The cumulative effect of the complex damage was again to lower the mode's group velocity, although for this case, the effect was produced by a different mechanism. For both studies, the array-type transducers used to excite and detect the waves were fabricated in the laboratory of Northwestern University.

2.1 SPECIMENS.

Specimen I is a carbon-epoxy, plain-weave, quasi-isotropic prepreg composite panel manufactured by Cytec Industries, Inc. with inserts in the mid-plane (figure 1). This specimen contains programmed damage to simulate defects. The panel has two sections, one with 16 plies and the other with 24, laid up in a $[0/45/-45/90]_{2S}$ and $[0/45/-45/90]_{3S}$ configuration, respectively. The transition between the 3.7 mm and 5.6 mm of the two sides occurs gradually, layer by layer, over 3.5 inches. Inserts of different types (2-ply pillow, 4-ply pillow, 0.005-in. Teflon, and 0.005-in. Grafoil, which is a pure natural graphite), with various diameters (1.5, 1, 0.75, 0.5, and 0.25 in.), were introduced in the panel's mid-plane during fabrication. Two additional rows of defects (0.5 and 1 in.) were inserted closely under the surface in the transition zone between the 16- and 24-ply sides of the panel. The *n*-ply pillow insert is a layered structure having *n* layers of tissue paper sealed in between two layers of 0.002-inch Kapton film. The specimen also contains flat-bottom holes of different sizes as well as pull-tabs that can be described as programmed semi-circular voids located near the edge of the specimen.

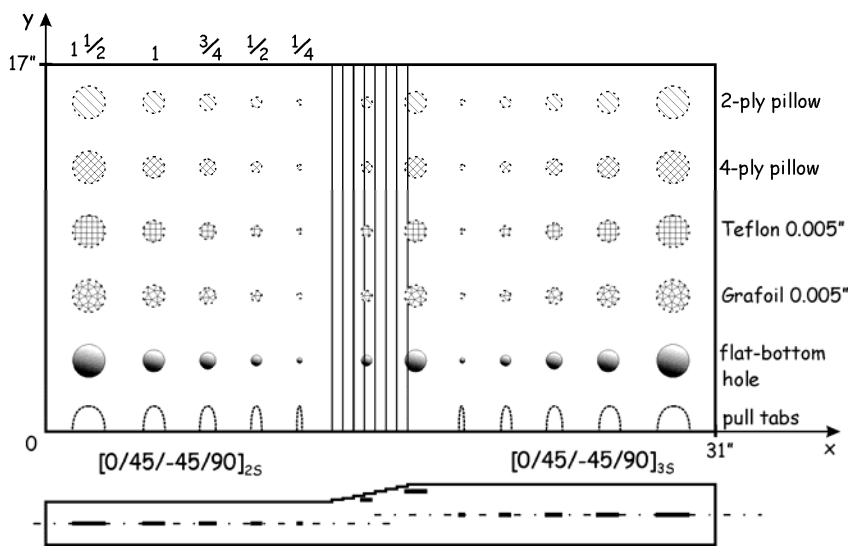

Figure 1. Specimen I, a Carbon-Epoxy, Plain-Weave, Quasi-Isotropic Composite Panel Reference Standard

Specimen II, used for impact, is a carbon-epoxy, cross-ply composite panel manufactured at the National Institute for Aviation Research, at Wichita State University. The panel is made of 24 plies, BMS 8-276, laid up in a $[0/90]_{6S}$ configuration. The total thickness of this panel is 4.6 mm. It should be noted that this material system and configuration is not necessarily

representative of actual composite structure in aircraft but instead was chosen for its wave propogation behavior, which is more easily characterized than a more complex example.

2.2 LAMB WAVES.

One of the defining characteristics of Lamb waves is their dispersive nature [10]. At a given frequency, a multitude of independent modes (≥2) can be excited. The number of modes increases as the frequency-thickness product (*fD*) increases. Each mode has a specific frequency-dependent displacement and stress profile through the thickness of the plate. Due to the differences in their propagation characteristics and profiles, different modes can be used to monitor different types of damage.

Excitation and detection of individual Lamb modes is possible through various techniques. In all cases, for a traveling wavepacket to maintain its shape over extended propagation distances, the excitation needs to be done at specific zones in the dispersion curves, namely where the dispersion is less pronounced. It is therefore helpful to know the details of the dispersion curves of the investigated material (or at least of a comparable material) before designing the appropriate modally selective transducers. The Lamb wave dispersion curves for the specimens used in the present experiments were calculated numerically using the classical transfer matrix method for layered media [11 and 12]. Figure 2 shows the dispersion curves for specimen I: woven $[0/45/-45/90]_{2S}$ and specimen II: cross-ply $[0/90]_{6S}$. The propagation direction of the waves is along the 0 direction. The symbols represent frequency (*f*) and plate thickness (*D*). The surrounding medium is assumed to be a vacuum. The shear-horizontal modes that were also obtained as solutions are not included in the figure. The material properties used in the calculations are given in table 1 (axis 1 is along the propagation direction). In the calculation, each layer was rotated according to the lay-up scheme. Note the 1<->2 and 2<->3 symmetry for the first and second specimens, respectively. For the woven specimen, the E_{11} modulus and the density were known from the manufacturer, while the other quantities are the typical values found for carbon-epoxy, plain-woven composite. For the cross-ply specimen, the numbers used are generic values that were obtained from the manufacturer for the type of prepreg used to fabricate the specimen.

The A_0 mode was chosen in the current investigation for several reasons: (1) the A_0 mode has an extended domain with minimal dispersion (at *fD* >0.2 MHz·mm), (2) the small wavelength of the A_0 mode (λ_0~4.5 mm for the given specimens) provides adequate resolution of detection, and (3) the A_0 mode is sensitive to defects located in the mid-plane. Generally, the S_0 mode can also be used in its low-dispersive region at low *fD* values. The S_0 mode has the additional benefit of lower attenuation, but the combination of high velocities and low frequencies produces wavelengths on the order of 40 mm, which can have an undesirable effect on the resolution of the measurements.

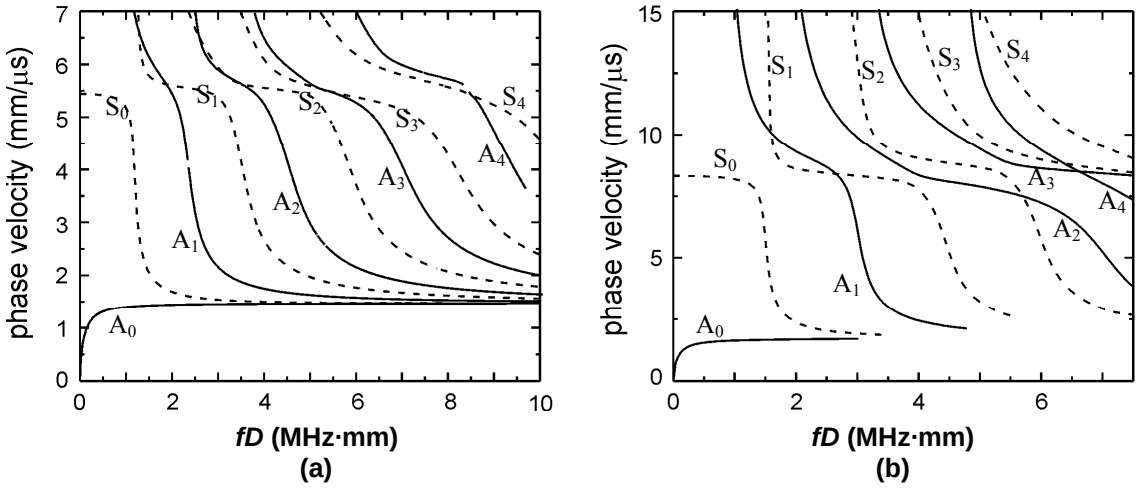

Figure 2. Numerically Calculated Phase Velocity Dispersion Curves for Lamb Waves in the Composite Materials Investigated, (a) Specimen I and (b) Specimen II

Table 1. Material Properties of a Layer Used in Calculating the Dispersion Curves of the two Specimens Used in the Experiments

Material Properties	E_{11} (GPa)	E_{22} (GPa)	E_{33} (GPa)	G_{12} (GPa)	G_{13} (GPa)	ν_{12}	ν_{13}	ν_{23}	ρ (kg/m^3)
Specimen I (woven)	61	61	9.65	4.48	3.45	0.044	0.08	0.08	1561
Specimen II (cross-ply)	206	11.3	11.3	6	6	0.34	0.34	0.5	1580

2.3 TRANSDUCERS.

The transducers used in this study were based on a concept widely used in surface acoustic-wave devices, namely, periodic arrays of coherent sources. Interdigital transducers designed for Lamb wave excitation and detection [13] in aluminum plates have been analyzed by Castaings, et al. [14], Monkhouse, et al. [15], and Rose, et al. [16]. In this work, a simple design was used, with a single set of fingers at the same potential instead of two sets driven at opposite phase. This eliminates the need for high-voltage radio frequency (RF) transformers. The fingers were spaced at a distance λ_0 apart. The piezoelectric material used was PVDF [17 and 18], a thin and flexible polymer that has certain advantages, such as a low profile, malleability, a low Q factor, and minimal cost. As discussed, these are important attributes for sensors intended to be used in SHM. The lower piezoelectric constant of PVDF (33 pm/V) versus that of other piezoelectrics (e.g., lead zirconate titanate (PZT), 590 pm/V) is partially compensated by a better transmission between the transducer and the composite specimen due to a better acoustic impedance match ($Z_{PVDF} = 2.5\text{x}10^5$ g/cm^{3}s).

A schematic of the transducers, showing both a top view and a cross-sectional view (expanded), is shown in figure 3. The PVDF film, which is 110 μm thick, is poled in the thickness direction (axis **3**) and has piezoelectric constants of d_{33} = -33 pm/V and d_{31} = 23 pm/V. Direction **1** was

chosen to coincide with the direction of wave propagation. In the actuator mode, an alternating current (AC) voltage applied between the electrodes and the grounded specimen creates an oscillating electric field with a strong component along direction **3**. Strains with periodicity λ_0 are induced within the piezoelectric material in directions **3** and **1**. The normal stresses (σ_{33}) applied to the specimen surface at the periodic location of the fingers and the shear stresses (σ_{13}) applied in between the fingers are the mechanical excitations that excite the plate waves. The Lamb mode, with its characteristic stress and displacement profiles, fully develops at a short distance away from the transducer. Since $d_{33} > d_{31}$, the modes with dominant normal surface displacement are more efficiently excited. Most modes can be excited, nonetheless. Note that the total thickness of the sensor of 0.3 mm (PVDF thin film plus metal electrode) is not tuned to resonate at a specific frequency. The reverse process takes place at the receiving transducer where an AC voltage is measured. If too weak, the received signal is further amplified. In some cases, an impedance-based matching network for the receiver or/and the source transducers was used to improve the signal-to-noise ratio (S/N). The S/N can be further improved if the PVDF is replaced with a stronger piezoelectric film, such as PZT fiber composites, also a flexible piezoelectric. However, that would increase the price of the sensors. The tests presented in this study were performed using PVDF transducers and no matching networks.

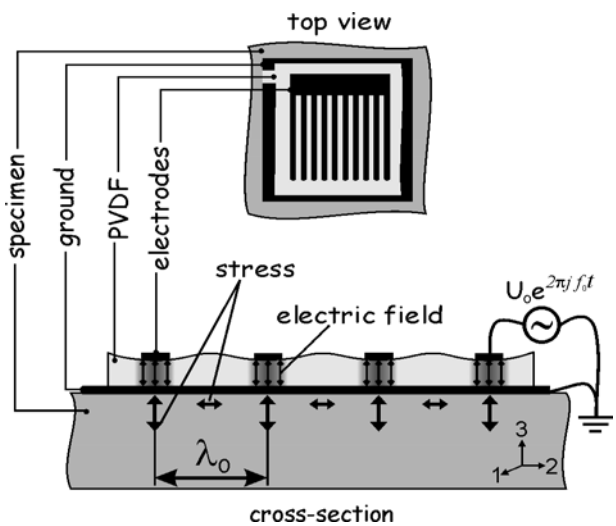

Figure 3. Top and Expanded Cross-Section Views of the Transducer

The number, width, and spacing of the electrode fingers control the central wavelength and bandwidth of the generated/detected wave. A general rule is that the total number of fingers controls the width of the central lobe and its amplitude. Increasing the number of fingers enables better modal selectivity, but the sensor lengths become unreasonably long. Apodization can also be used to manipulate the spectrum. Figure 4 shows the spatial spectra of an eight-finger pattern, with all fingers the same width ($\lambda_0/2$) and the finger widths apodized with a Hanning function. The solid curve shows all fingers have equal widths ($\lambda_0/2$), and the dashed line illustrates the finger widths are apodized with a Hanning function. The total number of fingers is eight, and the periodicity is $\lambda_0 = 4.5$ mm. U_0 is an arbitrary amplitude reference. In the apodized pattern, while the amplitude of the side lobes decreases compared to the central lobe, the width of the central

lobe, Δk, increases. For all the tests presented in this report, the same pair of nonapodized transducers were used, with wavelength $\lambda_0 = 4.5$ mm, $N = 8$ fingers, and $\Delta\lambda_0 = 0.8$ mm.

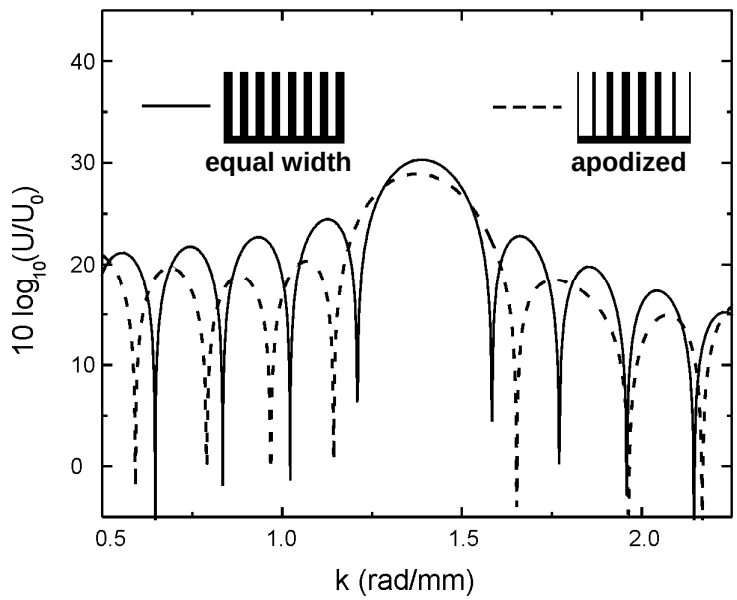

Figure 4. Spatial Distribution Spectrum of the Finger Electrodes as a Function of the Wave Number $k = 2\pi/\lambda_0$

The most important characteristic of these sensors is their mode-selection ability. For a given λ_0 (fixed by design), different modes can be excited/detected at different frequencies, according to $\lambda_0 = c_{phase}/f$ and the dispersion curves. The (c_{phase}, f) values of the chosen modes are preferably lying in a low-dispersion region, such that the modes propagate without distortion. An example is given in figure 5 for a pair of transducers with $\lambda_0 = 4.5$ mm mounted on the cross-ply specimen described in section 2.1. One mode is excited at 0.31 MHz and has a group velocity of 1.47 mm/µs. Another mode is excited at 1.27 MHz and has a group velocity of 2.98 mm/µs. Based on the (λ versus fD) and the group velocity versus fD curves, derived from the phase velocity data in figure 2(b) and considering the sensitivity of the dispersion curves to variations in the material properties, the two modes are identified as A_0 and A_2, respectively. The theoretical group velocities for A_0 and A_2 at the required frequencies are 1.75 and 3.6 mm/µs, respectively. The strong electromagnetic pickup between the source and receiver is observed when $t = 0$.

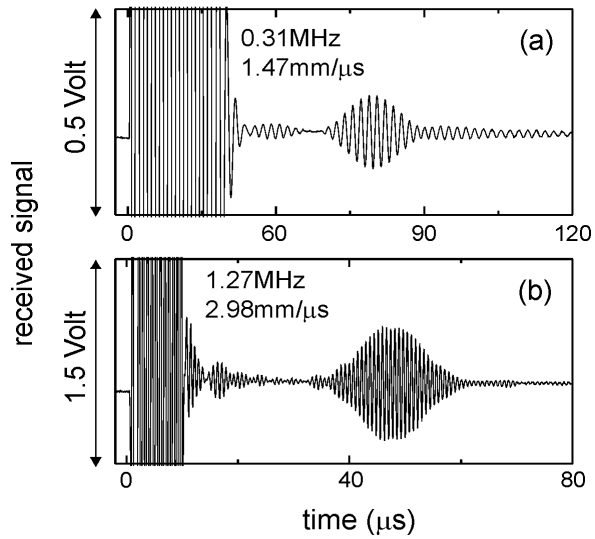

Figure 5. Two Different Modes Excited by the Same Pair of Transducers (λ_0 = 4.5 mm) at two Different Frequencies in the Cross-Ply Specimen

2.4 EXPERIMENTAL PROCEDURE.

A schematic diagram of the experimental setup using a pair of matched transducers is shown in figure 6. By reciprocity, the role of the source (S) and receiver (R) transducers can be reversed without any change in the results. The transducers were coupled to the specimen through a layer of honey, which is known to be a good shear wave couplant. For permanently installed sensors, conductive epoxy can provide both mechanical contact and a good ground electrode. A function generator and a gated RF amplifier were used to generate a 10-cycle tone burst with V_{RMS} = 115V. The composite panel was grounded at one corner. The signal picked up at the receiver was passed through the amplification stage of a Panametrics 5055 pulser/receiver and a low-pass, 2.5-MHz filter for noise reduction. The gain was set between 0 and 50 dB, depending on the amplitude of the signal received. The signals were viewed with an oscilloscope and were recorded for subsequent analysis. Since neither transducer was shielded, there was a large electromagnetic pickup between the source and the receiver that was visible in all the signals. The Lamb wave signal of interest was well separated in time from the electromagnetic interference signal. This interference is, in fact, a valuable reference indicator when comparing multiple time traces of ultrasonic signals.

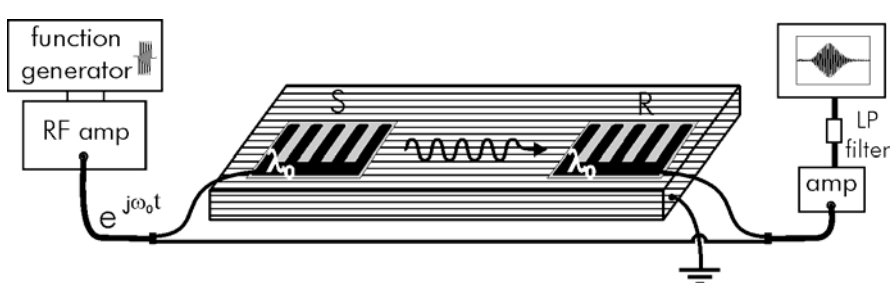

Figure 6. The Experimental Setup

3. DETECTION OF ARTIFICIAL DELAMINATIONS.

3.1 MODAL PURITY.

In the first experiment, the propagation characteristics of the A_0 mode were verified for the x and y directions (figure 1) of the woven composite panel (specimen I). The transducers were excited at frequency f = 0.31 MHz, and measurements were taken on the 3.7-mm-thick part of the panel. Keeping one transducer fixed, the other transducer was moved in increments of 1 cm at 15 different locations, gradually increasing the distance between the source and receiver from 5 cm to 19 cm. The time traces of the 15 signals received for the x direction are displayed in figure 7(a). The measurements for the propagation in the y direction were very similar. Note that the propagating mode was stable, maintaining its group velocity and shape over an extended propagation distance. The mode was also stable in the frequency domain. Frequency variations (±0.05 MHz) significantly affect the amplitude of the pulse while the shape of the pulse remains unchanged. Figure 7(b) shows the distance between the source and the receiver versus the peak-amplitude arrival time. The group velocity, estimated from the linear fit of distance versus peak-arrival data (figure 7(b)), is c_x = 1.586 mm/μs (fit correlation coefficient r_{cx}^2 = 0.9994). For the y direction, the linear fit yields c_y = 1.565 mm/μs (with r_{cy}^2 = 0.9996). The values measured for the group velocity correspond to what was expected for the A_0 mode in this material at this thickness and frequency (fD = 3.7 × 0.31 MHz·mm), based on the theoretical curve. Figure 7(c) shows $-ln(V_{pp})$ versus source-to-receiver distance. The attenuation of the wave can be estimated from linear curve fitting of $ln(V_{pp})$ versus the propagation distance (figure 7(c)), although the result may be error-prone due to variations in the couplant. The attenuation coefficients for the two directions were estimated as α_x = 0.226 Np/cm (fit correlation coefficient $r_{\alpha x}^2$ = 0.9966) and α_y = 0.207 Np/cm (with $r_{\alpha y}^2$ = 0.9982). From the results above, it follows that the propagation of the mode along x or y has very similar characteristics, as expected for this composite lay-up. The small measured differences are attributed to experimental errors and variations in the material properties.

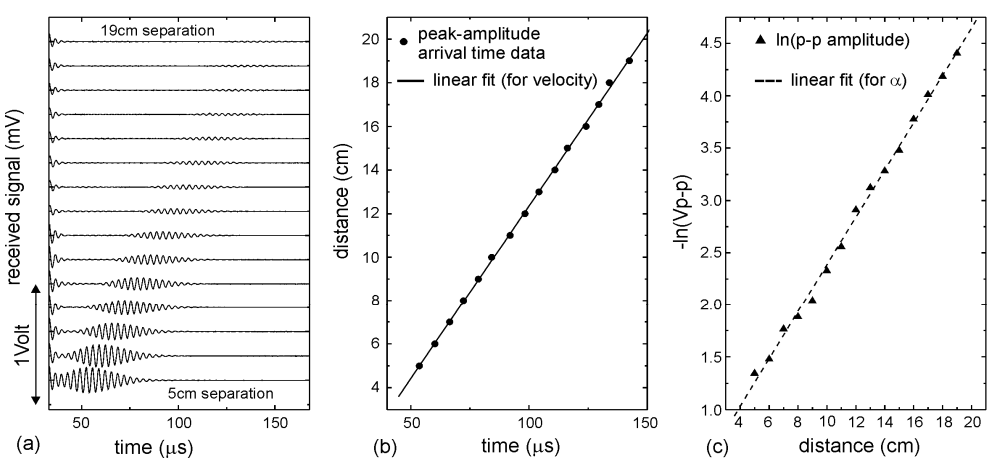

Figure 7. Propagation Characteristics of the Excited Mode Along the x Direction of the Composite Panel

3.2 RESULTS FOR ARTIFICIAL DELAMINATIONS.

Two types of scans were performed for the woven panel using the A_0 mode: type I, which examines inserts of the same type but different sizes, and type II, which examines inserts of the same size but different types. In type I scans, the transducers were translated in the x direction and the waves propagated in the y direction, as shown in figure 8. Measurements were taken when the center of the ultrasonic beam coincides with the center of the defect (1, 3, etc.), and when the center of the ultrasonic beam is equally distanced from two neighboring defects (2, 4, etc.). The opposite was the case for the type II scans. The received signals were recorded at specific locations of the transducers. The odd-numbered propagation paths, hereafter called across paths, pass directly through the defects. The even-numbered propagation paths, hereafter called not-across paths, are equidistant between two neighboring defects probing the "undamaged" composite. The distance between the edges of neighboring defects was 50 and 40 mm for the x and y directions, respectively. Great care was taken to maintain a constant distance between the source and the receiver, as this was crucial for the accuracy of the measurements. For each scan, two parallel guiding rails, secured to the panel, were used. At each measurement, the transducers were pushed flush against their associated rail and taped to the rail. Checks of parallelism between the two rails were done before and after the scans. No shifts were found. Variations in the source-receiver distance can also come from accidental gaps between the transducers and the rails. These are estimated to be a maximum of 0.2 mm. The 0.2-mm distance is equivalent to a time delay of 0.126 or 0.128 μs, depending on the propagation direction (x or y). This is the estimated error in the time delay measurements reported in figures 9 and 10. Note that, since the rails are on the outside of the monitored area, the measured time delay can only be underestimated with respect to the actual time delay.

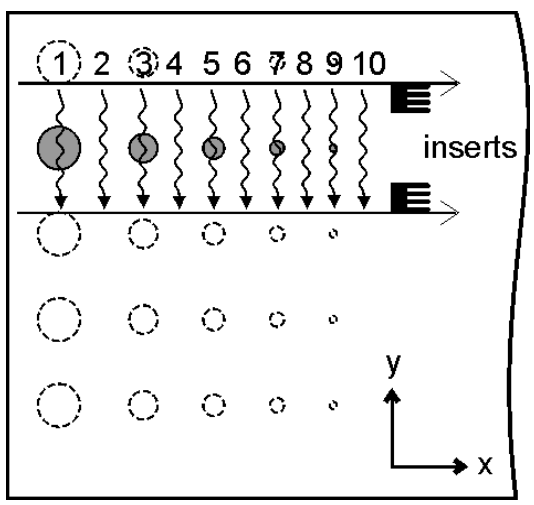

Figure 8. Type I Scan (Transducers are translated in the x direction; waves propagate along the y direction)

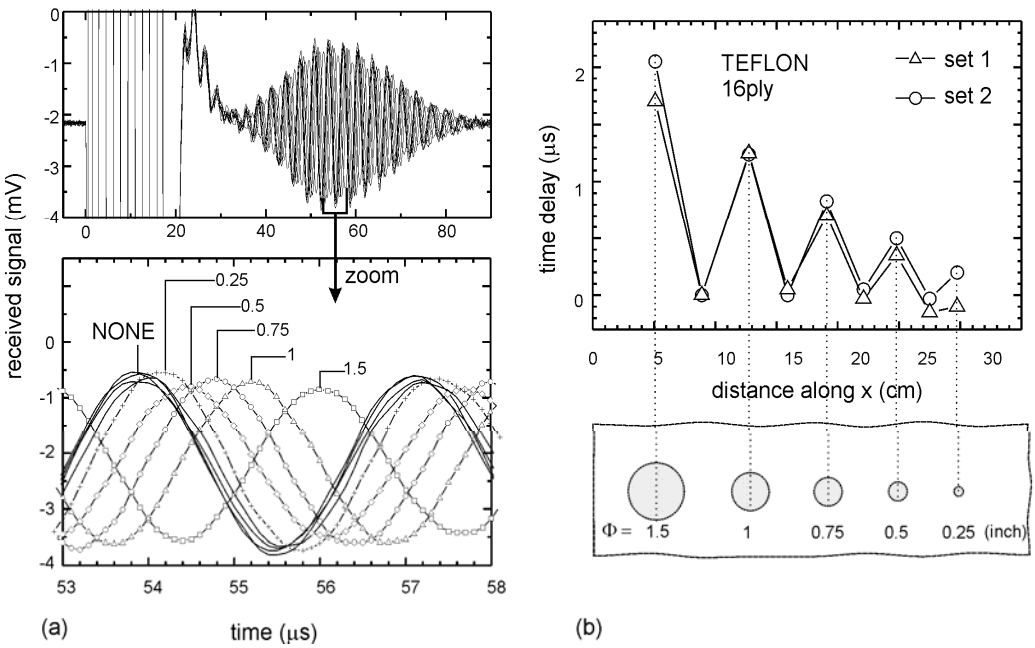

Figure 9. Type I Scan of the row of Teflon Inserts (from 1.5 to 0.25 in.) on the 3.7-mm Side of the Panel

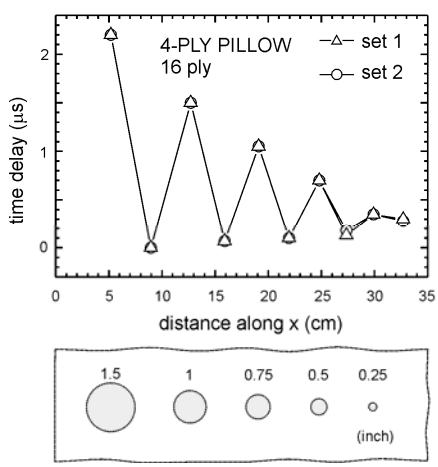

Figure 10. Type I Scan Time Delay Measurement of the 4-Ply Pillow Inserts on the 3.7-mm Side of the Panel

3.2.1 Scan of 3.7-mm-Thick Side, $[0/45/-45/90]_{2S}$.

A scan of type I was performed across the row of Teflon inserts. Time traces from 9 across and not-across paths (as described in section 3.2) are shown in figure 9(a) (full trace in the upper plot and zoom in the lower). While the signals from the across positions are consistently in phase, the signals from the not-across positions exhibit clear phase shifts, apparently correlated with the size of the defect. The electromagnetic pickup, in phase for all signals, is also visible. The time delay for each signal was calculated with the *xcorr* function of MATLAB®, using one off-the-defect position (position 2, at x = 9 cm) as reference. In the correlation, only the tone-burst part

of the time trace was used. Figure 9(b) shows the time delay calculated for the nine traces, using position 2 as reference. Two separate scans are plotted. The location of the inserts along the x direction is shown below the time delay plot. A similar set of measurements, taken under the same conditions but scanning the row of 4-ply pillow inserts, was performed. The results are displayed in figure 10. Time delay was calculated for 10 across and not-across traces using position 2 (x = 9 cm) as reference.

Type II scans were performed for the columns with 1-, 0.75-, and 0.5-in. inserts. The calculated time delay is plotted for all three sizes in figure 11. Time delay was calculated for 10 across and not-across traces using position 1 (x = 5 cm) as reference. Each point is the average of measurements taken during two separate scans. The location of the inserts along the y direction is shown below the plot. As in the type I tests, the data had very good reproducibility between the repeated scans.

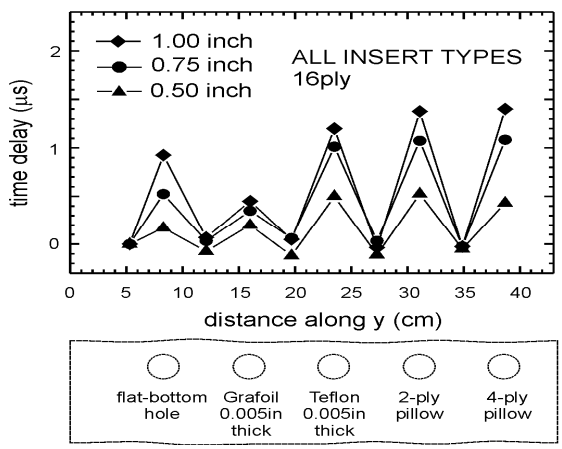

Figure 11. Type II Scan Time Delay Measurement on the 3.7-mm Side of the Panel

3.2.2 Scan of 5.6-mm-Thick Side, $[0/45/-45/90]_{3S}$.

Measurements were also taken at the thicker part (24 ply) of the panel. The A_0 mode was obtained again at f = 0.31 MHz. That is because the fD increase, due to a thicker plate, corresponds to only a slight change in the group velocity in this zone of the A_0 dispersion curve. One type I scan was performed for the row with Teflon inserts of different sizes, and one type II scan was performed for the column with 0.75-inch inserts of different types. The time delays for the two scans are plotted in figures 12 and 13. Note that the time delay was calculated for 10 across and not-across traces using position 2 (x = 9 cm) and position 1 (x = 4 cm) as reference for figures 12 and 13, respectively.

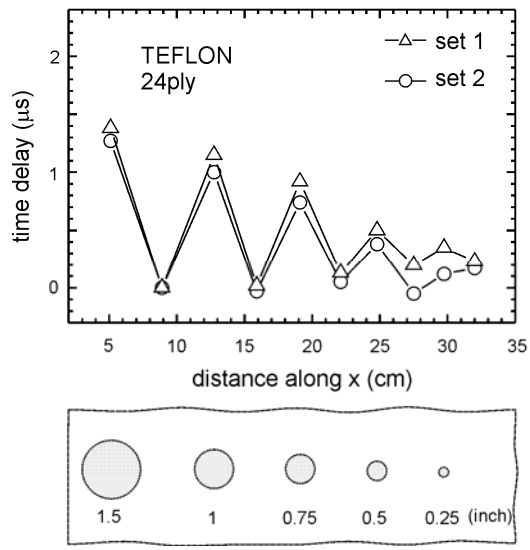

Figure 12. Type I Scan Time Delay Measurement of the Teflon Inserts Row (sizes from 1.5 to 0.25 in.) on the 5.6-mm Side of the Panel

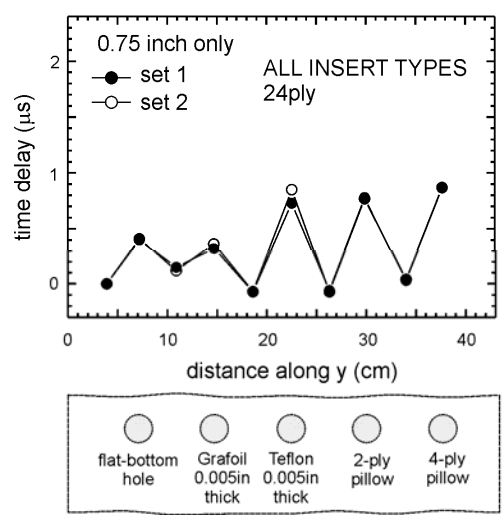

Figure 13. Type II Scan Time Delay Measurement of the Column With 0.75-Inch Inserts of Different Types on the 5.6-mm Side of the Panel

3.3 ANALYSIS.

A simple analysis was performed that indicated the reasons for the observed time delays. In regions where the composite panel was undamaged, the wave propagated with minimal dispersion at the chosen *fD* value at which it was excited. As the wave reached the area where the insert separated the panel in two symmetric sections with half the original thickness and (ideally) with free surfaces, the wave was forced to propagate through the two adjoining sections with half the original *fD*. The wave velocity at $fD_{1/2}$ was slightly lower, which caused the time

delay in the received pulse. Subsequent to the defect region, the wave continued to propagate at the velocity corresponding to the original *fD* value. Clearly, the time delay depends on the size and shape of the defect. If a relationship can be established between them, then a quantitative evaluation of the defect can be done. To verify that the time delay observed is truly a measure of the size of the defect (assuming the same type defect), a simple calculation can be carried out based on the geometry shown in figure 14. Note that Φ <2w in this figure. In the experiment, 2w = 20 mm; two of the defects (1.5 and 1 in.) span an area wider than 2w.

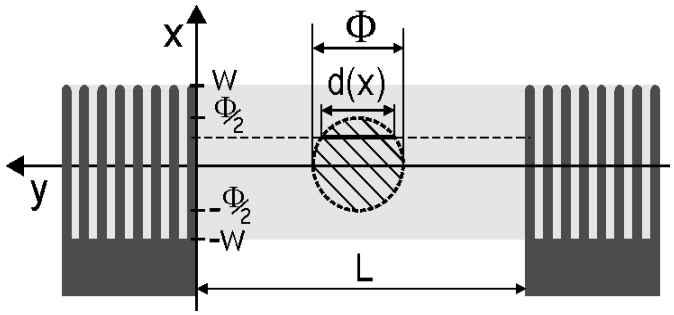

Figure 14. Geometry Used for Calculating the Velocity at Half Plate From the Observed Time Delay and the Defect Diameter

The transducers span an area which is 2w wide along the x axis (w = 10 mm in the experiment). Considering the ray indicated by the dashed line in figure 14, the time delay of the signal propagating along that ray is given by

$$\Delta t(x) = \frac{d(x)}{c_{1/2}} - \frac{d(x)}{c} \tag{1}$$

where Φ is the defect diameter, c is the velocity at *fD*, $c_{1/2}$ is the velocity at $fD_{1/2}$, and *d(x)* is the distance traveled across the delamination, $d(x) = 2\sqrt{(\Phi/2)^2 - x^2}$. Averaged over the diameter of the defect (or the width of the active area of the transducers when the defect exceeds that area), the average time delay by all rays between the generating and receiving transducers becomes

$$\Delta t = \begin{cases} \dfrac{1}{\Phi}\displaystyle\int_{-\Phi/2}^{\Phi/2} d(x)\left(\frac{1}{c_{1/2}} - \frac{1}{c}\right)dx = \frac{\pi}{4}\left(\frac{1}{c_{1/2}} - \frac{1}{c}\right)\Phi, \quad \Phi \le 2w \\ \dfrac{1}{2w}\displaystyle\int_{-w}^{w} d(x)\left(\frac{1}{c_{1/2}} - \frac{1}{c}\right)dx = w\left(\frac{1}{c_{1/2}} - \frac{1}{c}\right)\left[\sqrt{\left(\frac{\Phi}{2}\right)^2 - w^2} + \left(\frac{\Phi}{2}\right)^2 \sin^{-1}\left(\frac{2w}{\Phi}\right)\right], \quad \Phi \ge 2w \end{cases} \tag{2}$$

Due to scattering and beam nonuniformity for $x \in [-\Phi/2, \Phi/2]$, as well as diffraction and beam spreading, the variation of the signal amplitude was not considered in this calculation. The velocity along the y direction of the panel was measured as c = 1.565 mm/μs at full thickness D. Equation 2 can be used for two purposes. If Φ is known, $c_{1/2}$ can be calculated using the

measured time delay. Conversely, if $c_{1/2}$ is known, Φ can be determined. Equation 2 is applied to determine the size of the various 4-ply pillow defects for which the time delay was measured (figure 10). First, $c_{1/2}$ was calculated as $c_{1/2}$ = 1.417 mm/μs by using the measurements corresponding to one of the defects (Φ = 1 inch). It was expected that $c_{1/2}$ would be the same for all defects of the same type. The 1-inch defect was chosen since the value obtained for $c_{1/2}$ is the closest to the mean value of $c_{1/2}$ calculated using all the defects. Variation from the mean of $c_{1/2}$ calculated using the 1.5-, 1-, 0.75-, 0.5-, and 0.25-in.-diameter defects are 1.00%, -0.04%, -0.42%, -0.30%, and -0.23%, respectively. Next, using this value of $c_{1/2}$, the sizes of the other defects were estimated from the measured time delays. The calculated diameters of all the defects are given in table 2.

Table 2. Defect Diameter Φ Calculated From the Time Delay Measurements for the 4-Ply Pillow Defects and the 16-Ply Teflon Defects

(a) 4-Ply Pillow Defects					
Defect diameter Φ (in.)	1.50	1.00	0.75	0.50	0.25
Time delay Δ*t* (average) (μs)	2.16	1.50	1.04	0.68	0.34
Calculated defect diameter (mm)	34.38	25.4	19.82	13.05	6.48
(in.)	1.35	1	0.78	0.51	0.26
Difference (%)	9.8	0	4	2.8	2
(b) 16-Ply Teflon Defects					
Defect diameter Φ (in.)	1.50	1.00	0.75	0.50	0.25
Time delay Δ*t* (average) (μs)	1.87	1.24	0.76	0.42	0.05
Calculated defect diameter (mm)	37.72	23.73	19.05	10.58	1.24
(in.)	1.48	0.93	0.75	0.42	0.05
Difference (%)	1.0	6.6	0	16.7	80.4

This analysis was also applied to determine the size of the Teflon defects from the measured time delay (figure 9). Again, $c_{1/2}$ was calculated from the Φ = 0.75-inch defect, for the same reasons as before. Using this value for $c_{1/2}$, the diameters of the other Teflon defects were calculated. The results are given in table 2. The 0.25-inch defect was not included in the $c_{1/2}$ average since it appears to be an outlier. This is observed better in the results (figure 9(b)), where the consistency of the results between two sets of measurements is weakest for the 0.25-inch defect.

3.4 DISCUSSION.

The results obtained for the 24-ply side of the panel show consistently smaller time delays for a given size and type of defect than those observed for the 16-ply side. This further strengthens the argument used to estimate the diameter of the defects from the velocity at $fD_{1/2}$. As the A_0 mode dispersion curve asymptotically approaches its limit at $fD \rightarrow \infty$, the difference between the velocity c at fD and $c_{1/2}$ at $fD_{1/2}$ becomes increasingly smaller, which results in a smaller time delay.

A more subtle point is raised by the results of the type II scans. Although the defects have the same size, a clear and consistent variation in the time delay was observed between defects of different types. The lowest values are obtained for the Grafoil inserts. A possible explanation for these variations is that the surface in the mid-plane, where the insert is located, is not the

ideal free surface that was considered in the simple analysis. The Grafoil insert has the closest acoustic impedance of all candidate materials to that of the composite material, and it therefore provides the largest deviation from the free surface condition. The 4- and 2-ply inserts, which contain a small amount of trapped air, provide a close-to-free surface at mid-plane, being the closest imitation of a real delamination.

4. DETECTION OF IMPACT DAMAGE.

The following sections present the preliminary results, indicating that the same approach described in sections 2 and 3 can be used effectively for detection and estimation of actual impact damage in the cross-ply specimens.

4.1 MODAL PURITY.

The ultrasonic measurements on the cross-ply specimen were done for one propagation direction (the fiber direction of the first layer) and the characteristics of the A_0 mode were verified for that direction only. The mode was checked at 13 source-to-receiver distances. In terms of mode stability, as a function of both propagated distance and frequency, a very similar evolution to that observed for the woven panel (figure 7) was found. The group velocity was measured as $c = 1.467$ mm/μs (fit correlation coefficient $r_c^2 = 0.9985$) and the attenuation coefficient was $\alpha = 0.1958$ Np/cm (fit correlation coefficient $r_\alpha^2 = 0.9995$) for the propagation direction along the fibers of the first layer.

4.2 RESULTS FOR IMPACT DAMAGE.

Coupons (1.5 by 12 inches) were cut from the cross-ply specimen, with the 12-in. side parallel to the fiber direction of the first layer. The transducers were mounted 90-mm apart. A 1-inch-radius steel ball was used as the impactor. Circular 100-g weights were attached to the ball and placed on a long screw that was securely connected to the ball. The energy of the impact was varied by changing the mass or the height of the falling impactor. A guiding rail was used to control the location of the impact with an estimated precision of 2 mm. The impact was applied with a constant energy of 22 J at the same point, 30 consecutive times. The time traces of the received signal (A_0 mode) recorded after each impact are shown in figure 15(a). The top trace corresponds to no damage. Measurements were taken after each impact and are shown in sequence. Plots of the amplitude and time delay of the pulse, as a function of the number of impact events, were extracted from the time traces and are shown in figure 15(b) for two impact energies. The time delay is directly related to the amount of damage. The amplitude, however, follows a less intuitive path. It first grows slightly with the increase of damage, after which it quickly starts to decrease, followed by another slight increase and a slow decrease. The results for time delay and amplitude obtained for another impact at 28-J energy are also shown in figure 15(b). The amplitude follows an unpredictable trend possibly because of the closing and opening of the delaminated regions with subsequent impact. This further confirms the necessity of using a damage parameter other than the signal amplitude that can be used to monitor the existence and amount of damage.

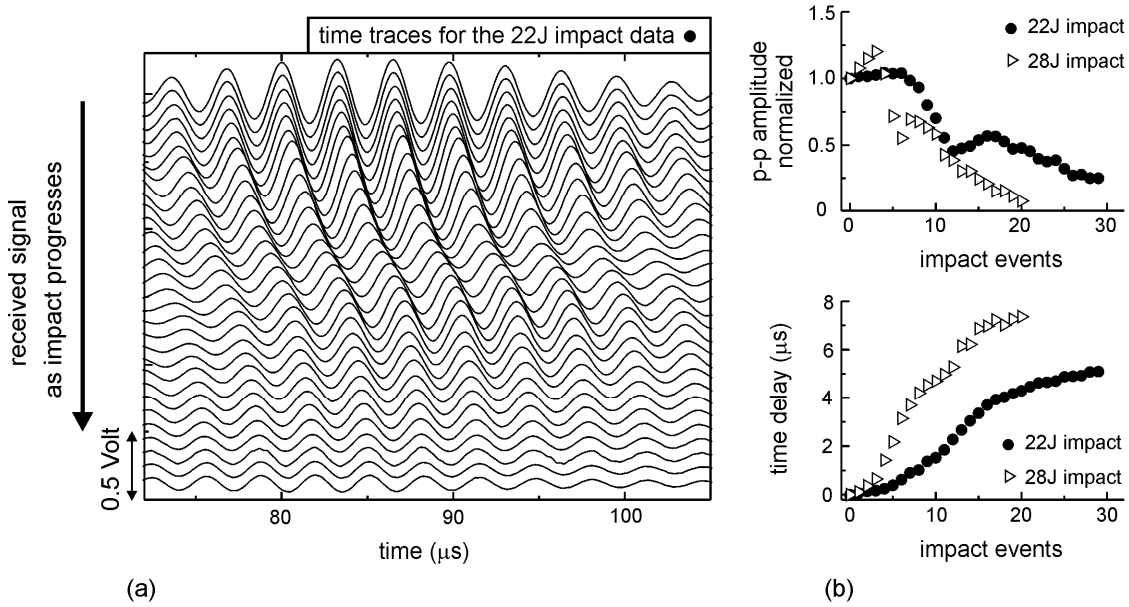

Figure 15. (a) Time Traces of the Received Signal in the 22-J Impact Test and (b) the Amplitude and Time Delay of the A_0 Pulse Measured as a Function of the Number of Impacts

A C-scan of the damaged coupon was taken after all impacts and is shown in figure 16.

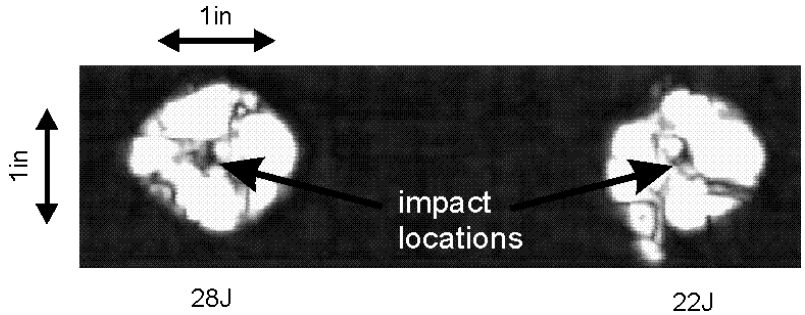

Figure 16. Ultrasonic C-Scan Image of the Impacted Cross-Ply Coupon in the Damaged Area at the Location of the two Hit Points (28 J and 22 J)

4.3 DISCUSSION.

The impact damage created in the composite is much more complex. It involves not only delaminations at multiple interfaces, but also matrix and fiber damage. The overall effect appears to be consistent with lowering the effective material stiffness, which results in a lower velocity (and therefore an increasing time delay). When the impact is applied at the same spot, the damage accumulates, although not necessarily in a linear fashion. For the two impact loads, the rate of increase of the time delay with the number of impact events appears to have the same trend, with a faster accumulation of damage for the larger load. An empirical relationship between the measured time delay and the size of the damage can be obtained from a C-scan image showing the size of the damaged area after each impact event. Empirical methods to correlate the time delay with the degree of damage are, at present, the best approach for the

quantitative determination of impact damage; this is because the details of the process that led to a decrease in stiffness, plus other mechanisms that contribute to lowering the wave velocity, are not yet well understood. If multiple modes are used for inspection (one at a time), it is expected that the damage will affect different modes to different degrees, a fact that could be used to further improve the ability to characterize the damage [19].

5. CONCLUSION.

A matched pair of modally selective transducers was fabricated and used to generate and receive a tone-burst Lamb wavepacket. When the wavepacket travels through a damaged region, the group velocity changes, causing a time delay in the received wavepacket. Two sets of experiments were performed to detect and size simulated delaminations and impact damage in graphite-epoxy laminated plates. Simulated delaminations were detected and their size was correctly estimated based on the measured damage parameter, the time delay. It was shown that time delay is a more robust measure of damage than signal attenuation. A simple ray analysis, taking into account the change in group velocity (induced geometrically by the defect), accurately accounts for the measured time delays. In addition, a similar exercise indicated that the proposed time delay damage parameter can also be used for real damage induced by impact. In this case, it was shown that the time delay damage parameter indicated a more stable, predictable result, when compared to amplitude variation as a damage parameter. It should be noted that the specific depth location of the defects will have a bearing on the ability to identify and size these defects using a specific Lamb mode. Since the Lamb wave modal distribution of energy is different at different operating points (mode-type as well as frequency), the sensitivity to the presence of defects will change. It will, therefore, be essential to design tunable, mode-selective transducers that can effectively probe the entire thickness of the plate. Ultimately, it is expected that such matched pairs of tunable, mode-selective Lamb wave transducers can be used for in situ structural health monitoring of composite laminates. While the laboratory test results were promising, future work in this area would need to be scaled up by considering more realistic damage sizes as well as more representative composite structure used in real aircraft designs. Addressing these issues would bring SHM technology closer to the necessary level so that it may be used as a tool for monitoring damage accumulation in composite aircraft structure.

6. REFERENCES.

1. Worlton, D.C., "Experimental Confirmation of Lamb Waves at Megacycle Frequencies," *Journal of Applied Physics*, Vol. 32, 1961, pp. 967-71.

2. Chimenti, D.E., "Guided Waves in Plates and Their use in Materials Characterization," *Applied Mechanics Reviews*, Vol. 50, 1997, pp. 247-84.

3. Alleyne, D.N. and Cawley, P., "The Interaction of Lamb Waves With Defects," *IEEE Transaction on Ultrasonics, Ferroelectrics and Frequency Control*, Vol. 39, 1992, pp. 381-97.

4. Cawley, P., "The Rapid Nondestructive Inspection of Large Composite Structures," *Composites*, Vol. 25, 1994, pp. 351-7.

5. Mal, A.K. and Ting, T.C.T., *Wave Propagation in Structural Composites*, American Society of Mechanical Engineers Press, New York, 1988.

6. Cawley, P., "The Detection of Delaminations Using Flexural Waves," *NDT International*, Vol. 23, 1990, pp. 207-17.

7. Hinders, M.K. and McKeon, J.C.P., "Lamb Wave Tomography for Corrosion Mapping," *Proceedings of the 2nd Joint NASA/FAA/DoD Conference on Aging Aircraft*, Williamsburg, Virginia, 1998, pp. 732-40.

8. Hildebrand, B.P., Davis, T.J., Posakony, G.J., and Spanner, J.C., "Lamb Wave Tomography for Imaging Erosion/Corrosion in Piping," *Review of Progress in Quantitative Nondestructive Evaluation*, Vol. 18, 1999, pp. 967-74.

9. Demcenko, A., Zukauskas, E., Kazys, R., and Voleisis, A., "Investigation of Interaction of the Lamb Wave With Delamination Type Defect in GLARE Composite Using Air-Coupled Ultrasonic Technique," *Proceedings of Forum Acusticum*, Budapest, 2005, pp. 2817-22.

10. Viktorov, I.A., *Rayleigh and Lamb Waves: Physical Theory and Applications*, Plenum Press, New York, 1967.

11. Nayfeh, A.H., *Wave Propagation in Layered Anisotropic Media With Applications to Composites*, Elsevier Science, B V, Amsterdam, 1995.

12. Lowe, M.J.S., "Matrix Techniques for Modeling Ultrasonic Waves in Multilayered Media," *IEEE Transaction on Ultrasonics, Ferroelectrics and Frequency Control*, Vol. 42, 1995, pp. 525-42.

13. Mattiocco, F., Dieulesaint, E., and Royer, D., "PVF_2 Transducers for Rayleigh Waves," *Electronics Letters*, Vol. 16, 1980, pp. 250-251.

14. Castaings, M., Monkhouse, R.S.C., Lowe, M.J.S., and Cawley, P., "The Performance of Flexible Interdigital PVDF Lamb Wave Transducers," *Acustica-Acta Acustica*, Vol. 85, 1999, pp. 842-9.

15. Monkhouse, R.S.C., Wilcox, P.W., Lowe, M.J.S., Dalton, R.P., and Cawley, P., "The Rapid Monitoring of Structures Using Interdigital Lamb Wave Transducers," *Smart Materials and Structures*, Vol. 9, 2000, pp. 304–9.

16. Rose, J.L., Pelts, S.P., and Quarry, M.J., "A Comb Transducer Model for Guided Wave NDE," *Ultrasonics*, Vol. 36, 1998, pp. 163-9.

17. Gachagan, A., et al., "Generation and Reception of Ultrasonic Guided Waves in Composite Plates Using Conformable Piezoelectric Transmitters and Optical-Fiber," *IEEE Transaction on Ultrasonics, Ferroelectrics and Frequency Control*, Vol. 46, 1999, pp. 72-81.

18. Hay, T.R. and Rose, J.L., "Flexible PVDF Comb Transducers for Excitation of Axisymmetric Guided Waves in Pipe," *Sensors and Actuators A (Physical)*, Vol. A100, 2002, pp. 18-23.

19. Petculescu, G., Krishnaswamy, S., and Achenbach, J.D., "Selective Excitation of Lamb-Waves for Damage Detection in Composites," *Review of Progress in Quantitative Nondestructive Evaluation*, Vol. 25, 2006, pp. 979-84.